Spectral Modeling of Magnetohydrodynamic Turbulent Flows

J. Baerenzung
TNT/NCAR, P.O. Box 3000, Boulder, Colorado 80307-3000, U.S.A.
Université de Nice-Sophia Antipolis, CNRS UMR 6202,
Observatoire de la Côte d'Azur, B.P. 4229, 06304 Nice Cedex 4, France

H. Politano and Y. Ponty
Université de Nice-Sophia Antipolis, CNRS UMR 6202,
Observatoire de la Côte d'Azur, B.P. 4229, 06304 Nice Cedex 4, France

A. Pouquet
TNT/NCAR, P.O. Box 3000, Boulder, Colorado 80307-3000, U.S.A.

We present a dynamical spectral model for Large Eddy Simulation of the incompressible magnetohydrodynamic (MHD) equations based on the Eddy Damped Quasi Normal Markovian approximation. This model extends classical spectral Large Eddy Simulations for the Navier-Stokes equations to incorporate general (non Kolmogorovian) spectra as well as eddy noise. We derive the model for MHD and show that introducing a new eddy-damping time for the dynamics of spectral tensors in the absence of equipartition between the velocity and magnetic fields leads to better agreement with direct numerical simulations, an important point for dynamo computations.

PACS numbers: 47.27.E-, 47.27.em, 47.27.ep, 47.27.er

I. INTRODUCTION

Magnetic fields permeate the universe. If kinetic effects such as Hall current, ambipolar drift of anisotropic pressure tensor, may be prevalent at small scales, the large-scales can be described in the magnetohydrodynamic (MHD) approximation. For example, electric fields and ionospheric currents play a dynamic role in the evolution of the atmosphere above 100 km, and the input of energy from the magnetosphere during magnetic storms can affect the thermosphere and ionosphere on global scales.

MHD has many similarities with Navier–Stokes (NS) turbulence: recall the Batchelor analogy between vorticity and induction, both undergoing stretching through velocity gradients (see equation (6)). On that basis, one can conjecture that the energy spectrum will be of the Kolmogorov type, as in fact observed in numerical simulations of a decaying flow ([1] and references therein), as well as in the Solar Wind [2]. However, Iroshinkov and Kraichnan (IK hereafter) hypothesized that the slowing-down of nonlinear transfer by Alfvén waves would alter the energy spectrum [3], predicting a spectrum $\sim k^{-3/2}$, as recently observed in numerical simulations [4, 5, 6] and in Solar Wind observations [7]. The Lagrangian renormalized approximation also gives spectra compatible with the IK model [8]. These spectra are isotropic, but the presence of a strong quasi-uniform magnetic field $\mathbf{B_0}$ at large scale renders the dynamic anisotropic. One can compute exactly the reduced dynamics in that case [9], using weak turbulence theory; the emerging energy spectrum $\sim |\mathbf{k}_\perp|^{-\mathbf{2}}$, where $\mathbf{k}_\perp$ refers to wavevectors perpendicular to $\mathbf{B_0}$ (note that the isotropization of such a spectrum is compatible with the IK spectrum). Note also that a weak turbulence spectrum was observed in the magnetosphere of Jupiter [10], the evidence stemming from an analysis of Galileo spacecraft data. A weak turbulence spectrum also obtained as well in a large numerical simulation of MHD turbulence in three dimensions [6] at a magnetic Taylor Reynolds number of ~ 1700 at scales smaller than where the isotropic IK spectrum is observed.

Both the terrestrial and Jovian magnetospheric plasmas as well as the solar wind, the solar atmosphere, and the interstellar medium are highly turbulent conducting compressible flows sustaining magneto-acoustic wave propagation and a better understanding of their dynamics, leading for example to star formation, requires adequate tools for modeling them. Furthermore, there is currently a surge of interest for achieving an experimental dynamo (the growth of a seed magnetic field through fluid motions, see [11]). In the case of liquid metals, or the fluid core of the Earth [12, 13, 14] or the solar convection zone, the magnetic Prandtl number is very small (10^{-5} or less); hence, the dynamo instability occurs in a turbulent flow and modeling the turbulence in order to study this phenomenon is in order [15, 16].

There are few models for MHD (see e.g. the recent review in [17]), comparatively to the fluid case where the engineering community has been driving a vigorous research agenda. In that light, this paper aims at developing such a model, in the context of a spectral approach following the work of Chollet and Lesieur [18] for the fluid case, using two-point closure of turbulent flows. We give the basic equations in the next section and then move on in Section III to recall the EDQNM closure formulation for MHD. New triad relaxation times are introduced in Section IV and first tested in Section V. The case of a random flow for two values of the magnetic Prandtl number P_M are treated respectively in Section VI ($P_M = 1$) and Section VII ($P_M = 0.1$), and the deter-

ministic Orszag-Tang flow in three dimension is analyzed in Section VIII. Finally, Section IX is the conclusion and two technical appendices (A and B) are given at the end.

II. MAGNETOHYDRODYNAMIC EQUATIONS

Let us consider the Fourier transform of the velocity $\mathbf{v}(\mathbf{x},t)$ and the magnetic $\mathbf{B}(\mathbf{x},t)$ at wavevector $\mathbf{k}$:

$$\mathbf{v}(\mathbf{k},t) = \int_{-\infty}^{\infty} \mathbf{v}(\mathbf{x},t) e^{-i\mathbf{k}.\mathbf{x}} \mathbf{dx} \quad (1)$$

$$\mathbf{B}(\mathbf{k},t) = \int_{-\infty}^{\infty} \mathbf{B}(\mathbf{x},t) e^{-i\mathbf{k}.\mathbf{x}} \mathbf{dx}. \quad (2)$$

The MHD equations describe the time evolution of a conducting fluid velocity field coupled to a magnetic field. They derive from Maxwell's equations with the assumption that velocities are sub-relativistic, hence the displacement current can be neglected [19, 20]. In terms of the Fourier coefficients of the velocity and the magnetic components, the MHD equations with constant unit density read:

$$\left(\frac{\partial}{\partial t} + \nu k^2\right) \mathbf{v}(\mathbf{k},t) = \mathbf{t}^V(\mathbf{k},t) \quad (3)$$

$$\left(\frac{\partial}{\partial t} + \eta k^2\right) \mathbf{b}(\mathbf{k},t) = \mathbf{t}^M(\mathbf{k},t) \ , \quad (4)$$

with $\mathbf{k}\cdot\mathbf{v} = \mathbf{0}$ in the incompressible case and $\mathbf{k}\cdot\mathbf{b} = 0$ indicating the lack of magnetic monopoles in the classical approximation. Here, $\mathbf{b} = \mathbf{B}/\sqrt{\mu_0\rho_0}$ is the Alfvén velocity, with μ_0 the permeability, and ρ_0 the uniform density (taken equal to unity); η is the magnetic diffusivity, ν the kinematic viscosity, and $\mathbf{t}^V(\mathbf{k},t)$ and $\mathbf{t}^M(\mathbf{k},t)$ are bilinear operators for energy transfer written as:

$$\begin{aligned} t_\alpha{}^V(\mathbf{k},t) &= -iP_{\alpha\beta}(\mathbf{k})k_\gamma \sum_{\mathbf{p}+\mathbf{q}=\mathbf{k}} v_\beta(\mathbf{p},t)v_\gamma(\mathbf{q},t) \\ &\quad + iP_{\alpha\beta}(\mathbf{k})k_\gamma \sum_{\mathbf{p}+\mathbf{q}=\mathbf{k}} b_\beta(\mathbf{p},t)b_\gamma(\mathbf{q},t) \quad (5) \\ t_\alpha{}^M(\mathbf{k},t) &= -i\delta_{\alpha\beta}k_\gamma \sum_{\mathbf{p}+\mathbf{q}=\mathbf{k}} b_\beta(\mathbf{p},t)v_\gamma(\mathbf{q},t) \\ &\quad - i\delta_{\alpha\beta}k_\gamma \sum_{\mathbf{p}+\mathbf{q}=\mathbf{k}} b_\beta(\mathbf{q},t)v_\gamma(\mathbf{p},t) \ , \quad (6) \end{aligned}$$

with $P_{\alpha\beta}(\mathbf{k}) = \delta_{\alpha\beta} - k_\alpha k_\beta/k^2$ a projector that allows to take the pressure term of the velocity equation into account via the Poisson formulation. The magnetic Prandtl number is defined as $P_M = \nu/\eta$. Finally note that, in the absence of dissipation ($\nu = 0 = \eta$), the total energy $E_T = 0.5 < v^2 + b^2 >$, the correlation between the velocity and the magnetic field $H_C =< \mathbf{v}\cdot\mathbf{b} >$ and the magnetic helicity $< \mathbf{A}\cdot\mathbf{b} >$ (with $\mathbf{b} = \nabla\times\mathbf{A}$) are invariants of the ideal MHD equations in three dimensions.

III. SPECTRAL MODELING

A. The original EDQNM closure

The Large Eddy Simulation model (LES) derived in [21] (Paper I hereafter) is now extended to the MHD equations in its non-helical version (LES-P). As a first step, a spectral filtering of the equations is realized; this operation consists in the truncation of all veloctity and magnetic components at a wave-vector $\mathbf{k}$ such that $|\mathbf{k}| > k_c$ where k_c is a cut-off wavenumber. In an intermediate zone lying between k_c and $3k_c$ both kinetic and magnetic energy spectra are assumed to behave as power-laws followed by an exponential decrease:

$$E^V(k,t) = E_0^V k^{-\alpha_E^V} e^{-\delta_E^V k}, \quad k_c \le k < 3k_c \quad (7)$$

$$E^M(k,t) = E_0^M k^{-\alpha_E^M} e^{-\delta_E^M k}, \quad k_c \le k < 3k_c \ , \quad (8)$$

where α_E^V, δ_E^V, E_0^V, and α_E^M, δ_E^M, E_0^M, are evaluated at each time step of the numerical simulations, through a mean square fit of the resolved kinetic and magnetic energy spectra. In a second step one can write the modeled MHD equations as:

$$\left[\partial_t + \left(\nu\left(k|k_c,t\right) + \nu k^2\right)\right] v_\alpha(\mathbf{k},t) = t_\alpha^{V<}(\mathbf{k},t) \quad (9)$$

$$\left[\partial_t + \left(\eta\left(k|k_c,t\right) + \eta k^2\right)\right] b_\alpha(\mathbf{k},t) = t_\alpha^{M<}(\mathbf{k},t) \quad (10)$$

where the $<$ symbol indicates that the nonlinear transfers are integrated on the truncated domain such as $\mathbf{p}+\mathbf{q}=\mathbf{k}$ with $|\mathbf{p}|, |\mathbf{q}| < k_c$. The quantities $\nu\left(k|k_c,t\right)$ and $\eta\left(k|k_c,t\right)$ which are respectively called eddy viscosity and magnetic eddy diffusivity are expressed as:

$$\nu(k|k_c,t) = -\iint_{\Delta^>} \theta_{kpq} \frac{\left(S_2^V(k,p,q,t) + S_4^V(k,p,q,t)\right)}{2k^2 E^V(k,t)} dpdq \quad (11)$$

$$\eta(k|k_c,t) = -\iint_{\Delta^>} \theta_{kpq} \frac{\left(S_2^M(k,p,q,t) + S_4^M(k,p,q,t)\right)}{2k^2 E^M(k,t)} dpdq \quad (12)$$

(see Paper I for more details). Here the $S_i^{V,M}(k,p,q,t)$ terms (see Appendix A), correspond to the absorption terms of the Eddy Damped Quasi Normal Markovian (EDQNM) nonlinear transfer, leading in particular to turbulent eddy diffusivities (see e.g. [22] for the MHD case). $\Delta^>$ is the integration domain on k, p, q, triangles such as p and or q are larger than k_c and both p and q are smaller than $3k_c$.

Finally, to take into account the effect of the emission (eddy-noise) terms of the EDQNM nonlinear transfer (i.e. $S_1^V(k,p,q,t)$, $S_3^V(k,p,q,t)$, $S_1^M(k,p,q,t)$, and $S_3^M(k,p,q,t)$), we use a reconstruction field procedure which also enables to partialy rebuild the phase relationships between the three spectral components of each velocity and magnetic fields, as explained in Paper I [21].

B. First numerical tests

We first implemented our LES model with the EDQNM equations of Pouquet et al [23] (see also [22]). In this formulation the triad-relaxation time Θ_{kpq} (see Appendix A) takes three characteristic times into account:
- a (combined) dissipation time τ_D defined as:

$$\tau_D^{-1}(k) = (\nu + \eta)\, k^2 \ , \tag{13}$$

- a nonlinear time τ_S expressed as:

$$\tau_S^{-1}(k) = \lambda \left[\int_0^k q^2 \left[E^V(q) + E^M(q) \right] dq \right]^{\frac{1}{2}} \ , \tag{14}$$

- and an Alfvén time τ_A which reads:

$$\tau_A^{-1}(k) = \left(\frac{2}{3} \right)^{\frac{1}{2}} k \left[\int_0^k E^M(q) dq \right]^{\frac{1}{2}} \ . \tag{15}$$

This constitutes a straightforward generalization of the EDQNM closure to the case of MHD flows (see for example [24]) in which two new times, specifically the Alfvén time and the diffusion time built on magnetic resistivity, are incorporated in a phenomenological manner. A comparison of a simulation using this LES model (LES MHD I, or run **II** in Table I), with a DNS simulation (run **I** in Table I) is shown in Fig. 1 (see next section for more information on the numerical procedure). One sees that both the kinetic and magnetic energy spectra are overestimated by the model at scales close to the cut-off, indicative of an inadequate energy transfer in the model at these scales. When evaluating numerically the different eddy dampings using eqns. (13-15), one observes that the Alfvén time is almost one order of magnitude shorter than all other times, including the diffusion time at the smallest resolved scales (see [25]); this leads to an insufficient damping at the scales close to the cut-off. This is in part due to the dominance of the magnetic energy at large-scale; in that sense, it could be linked to the particular flow under study and parametric analyses of several flows will have to be performed in the future in order to fine-tune this MHD model. However, the discrepancy displayed in Fig. 1 could also be linked to the particular expression of eddy damping chosen in [23]. We are thus led to examine more closely the dynamics of energy transfer within the EDQNM framework.

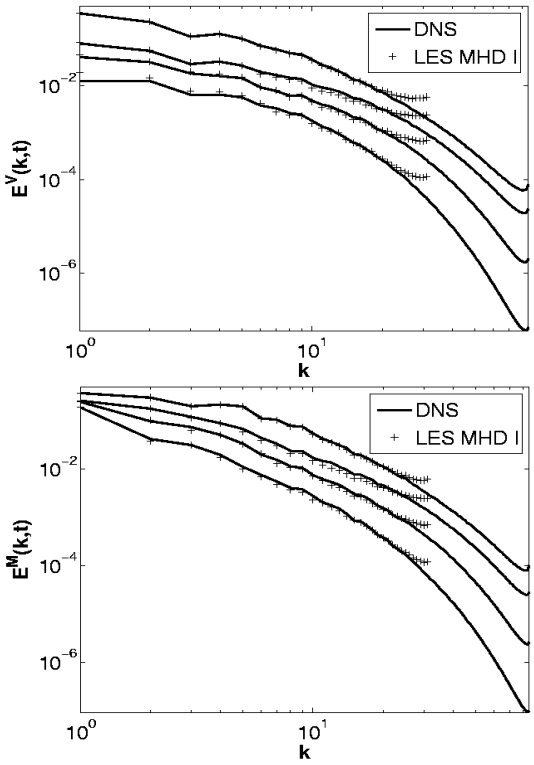

FIG. 1: Kinetic (top) and magnetic (bottom) energy spectra at time $t = 1$, $t = 3$, $t = 5$, and $t = 10$ from upper to lower curves for data **I** (256^3 DNS, solid line), and data **II** (64^3 LES MHD I, plus symbols).

IV. NEW RELAXATION TIMES FOR EDQNM

We now analyze the precise structure of the equations leading to the EDQNM closure; this is done in Appendix B. Note that a similar but more complex and systematic approach can be found in [8] in the context of the Lagrangian renormalization approximation. Our analysis results in the expression of three new eddy diffusivity times, with which one can build four different eddy-damping rates μ_{kpq}, namely:

$$\begin{aligned}
\mu_{kpq}^{VV} &= \tau_D^{VV^{-1}}(k,p,q) + \tau_{NL}^{-1}(k,p,q) \ , \\
\mu_{kpq}^{VM} &= \tau_D^{VM^{-1}}(k,p,q) + \tau_{NL}^{-1}(k,p,q) + \widetilde{\tau}_A^{-1}(k,p,q) \ , \\
\mu_{kpq}^{MV} &= \tau_D^{MV^{-1}}(k,p,q) + \tau_{NL}^{-1}(k,p,q) + \widetilde{\tau}_A^{-1}(k,p,q) \ , \qquad (16) \\
\mu_{kpq}^{MM} &= \tau_D^{MM^{-1}}(k,p,q) + \tau_{NL}^{-1}(k,p,q) + \widetilde{\tau}_A^{-1}(k,p,q) \qquad (17)
\end{aligned}$$

where:

$$\begin{aligned}
\tau_{NL}^{-1}(k,p,q) &= \tau_{NL}^{-1}(k) + \tau_{NL}^{-1}(p) + \tau_{NL}^{-1}(q) \ , \qquad (18) \\
\widetilde{\tau}_A^{-1}(k,p,q) &= \widetilde{\tau}_A^{-1}(k) + \widetilde{\tau}_A^{-1}(p) + \widetilde{\tau}_A^{-1}(q) \ . \qquad (19)
\end{aligned}$$

with $\widetilde{\tau}_A^{-1}(k,p,q)$ based on a new Alfvén-like time, namely

$$\widetilde{\tau}_A^{-1}(k) = C_A \left(\frac{\int_0^k E^M(q) dq}{\int_0^k E^V(q) dq} \right)^{\frac{1}{2}} \left[\int_0^k q^2 E^M(q) dq \right]^{\frac{1}{2}} . \tag{20}$$

Finally, from these eddy-damping rates we derive the corresponding triad-interaction times (as defined in Appendix A). For the EDQNM kinetic energy equation, we obtain two different Θ's, Θ_{kpq}^{VV} applied to $S_1^V(k,p,q,t)$ and $S_2^V(k,p,q,t)$, and Θ_{kpq}^{MM} applied to $S_3^V(k,p,q,t)$ and $S_4^V(k,p,q,t)$.

For the EDQNM magnetic energy equation we also obtain two triad-interaction time, namely Θ^{MM}_{kpq} applied to $S^M_1(k,p,q,t)$ and $S^M_2(k,p,q,t)$ and Θ^{MV}_{kpq} applied to $S^M_3(k,p,q,t)$ and $S^M_4(k,p,q,t)$. Note that this formulation leads to distinguish between the Joule and the viscous dissipation more systematically than in [23], and therefore to possibly better simulate flows at magnetic Prandtl numbers different from unity. Another difference is the special treatment of the Lorentz force in the velocity equation. We call LES MHD II the model that takes these new triad-relaxation times into account.

V. NUMERICAL SET-UP

In order to assess the ability of the model to reproduce the physics involved in MHD flows, we performed Direct Numerical Simulations (DNS) of the three-dimensional MHD equations, at a resolution of 256^3 grid points, together with computations based on our LES MHD formulation, but now using 64^3 grid points. We performed this comparative study from three different simulations of freely decaying MHD flows. To test our model in a simple configuration, we first run a simulation at $P_M = 1$ with random initial conditions and no correlation between the velocity and the magnetic field (run **I** for the DNS, run **II** for the LES MHD I, and run **III** for the LES MHD II, in Table I). Since the new eddy-damping times we derived allow for a clear distinction between the kinematic viscosity and the magnetic dissipation, we then simulated a flow with identical initial conditions but with now $P_M = 0.1$ (run **IV** for the DNS, and run **V** for the LES MHD II in Table I). We recall that, in the work of [23], the EDQNM closure has been derived for the case when the cross-correlation (or cross-helicity) spectrum $H^C(k) =< \mathbf{v}(\mathbf{k}) \cdot \mathbf{b}(\mathbf{k})(k) >$ is assumed to be identically zero in the presence of helicity (see [1, 26] for the non helical case in the presence of velocity-magnetic field correlation). However, for many flows, this quantity is non negligible; furthermore, it can be strong locally (in particular in the vicinity of vorticity and current sheets) even when the global correlation is close to zero [27, 28]. We thus performed as well a simulation at $P_M = 1$ for which the velocity and the magnetic field are significantly correlated, in order to see how our model may adapt to such a situation. We chose the so-called three-dimensional Orszag-Tang flow (run **VI** for the DNS, and run **VII** for the LES MHD II in Table I) for which initially $2H^C/E^T = 0.5$.

From all these simulations, we studied global flow quantities such as the total, kinetic and magnetic energies, as well as helicities, and the cross-correlation energy. We also analyzed the spectral behaviors of these quantities.

TABLE I: Parameters of the simulations. Initial conditions I.C., grid resolution N, kinematic viscosity ν, and magnetic Prandtl number $P_M = \nu/\eta$, with η the magnetic diffusivity.

		I.C.	N	ν	P_M
I	DNS	Random	256	$2.e^{-3}$	1
II	LES I	Random	64	$2.e^{-3}$	1
III	LES II	Random	64	$2.e^{-3}$	1
IV	DNS	Random	256	$8.e^{-4}$	0.1
V	LES II	Random	64	$8.e^{-4}$	0.1
VI	LES I	Random	64	$8.e^{-4}$	0.1
VII	DNS	OT	256	$2.e^{-3}$	1
VIII	LES II	OT	64	$2.e^{-3}$	1

VI. RANDOM FLOW AT $\mathbf{P_M = 1}$

We first investigate the model behavior for a flow with random initial conditions, presenting no cross-correlation, and at magnetic Prandtl number of unity.

A. Inter-comparison of models

In this section, we compare the efficiency between the model that involves the eddy damping times stemming from [23] (LES MHD I), and the model where the new eddy-damping times derived in Appendix B are included (LES MHD II). In Figure 2, we plot the relative difference of the kinetic and magnetic energy spectra computed from both LES models with the ones computed from the DNS. The spectra are chosen at time $t = 1$, close to the time of maximum dissipation.

At large scales (bewteen $k = 0$ and $k \simeq 15$) the LES MHD II model globally gives a better approximation of the kinetic and magnetic energy spectra. Bewteen $k = 14$ and $k = 20$ for the kinetic energy spectra, and between $k = 15$ and $k = 25$ for the magnetic energy spectra, the LES MHD I seems to give better results. This is due to the fact that LES MHD I and DNS spectra cross at a wavenumber located inside these ranges. Finally, at small scales, the LES MHD II data lead to a much better approximation than the LES MHD I data. At different times, the comparison between LES MHD I and LES MHD II results leads to similar results (not shown). We therefore focus our study on the LES MHD II model for the remainder of the paper.

B. Global quantities

We here study the time evolution of the global kinetic, $E^V(t)$, and magnetic, $E^M(t)$, energies for runs **I** and **III**, as shown in Figure 3).

One can observe that the modeled kinetic and magnetic energies both closely follow the DNS evolutions, although at short times (between $t = 1$ and $t = 5$ for

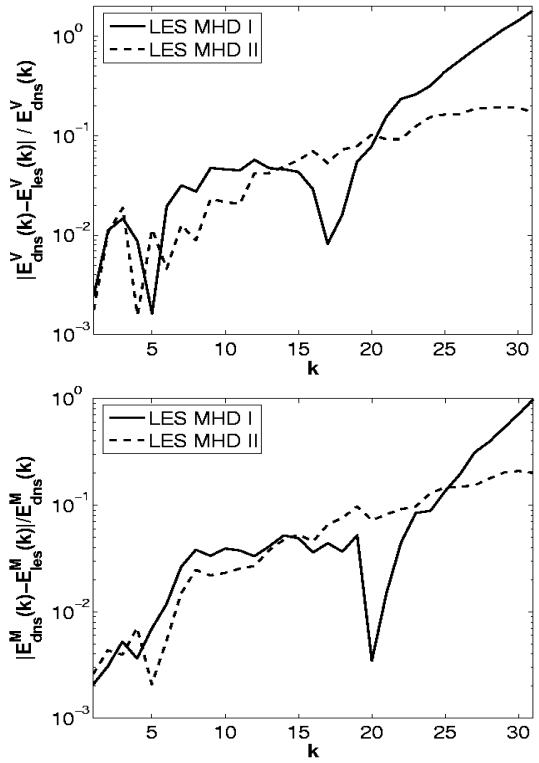

FIG. 2: Lin-log plots of the relative difference with DNS energy spectra for the velocity (top) and the magnetic field (bottom) at time $t = 1$, for runs **II** and **III**, compared to the DNS, run I. Note the large error in LES I at large k.

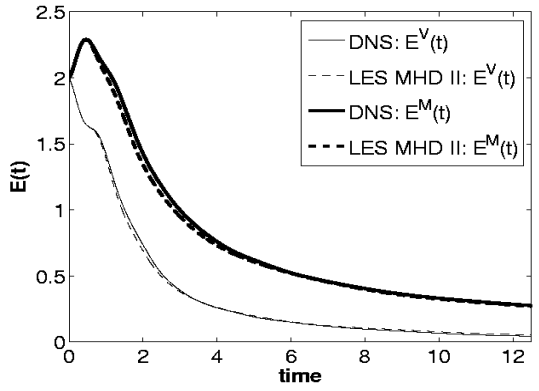

FIG. 3: Temporal evolution of the kinetic and magnetic energy for runs **I** (256^3 DNS), and **III** (64^3 LES MHD II).

$E^M(t)$ and between $t = 1$ and $t = 3$ for $E^V(t)$), the model slightly under-estimates them.

Since our field-reconstruction procedure uses the flow (kinetic and magnetic) helicities (even though the model itself does not take into account at this stage the helical contributions to evaluate the transport coefficient), we plot in Fig. 4 the time evolution of both kinetic and magnetic helicities (respectively $H^V(t)$ and $H^M(t)$).

One can notice that, even though both modeled kinetic and magnetic helicities do not exactly match the DNS

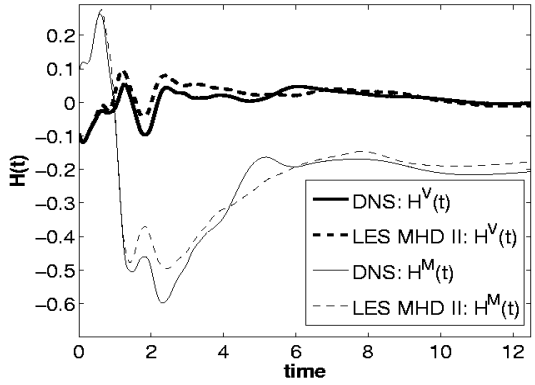

FIG. 4: Time evolution of the kinetic and magnetic helicities for runs **I** (256^3 DNS), and **III** (64^3 LES MHD II).

results at each time, they remain close and reproduce the main DNS time fluctuations. Note that the LES MHD I model provides similar results.

We do not present here the temporal evolution of the cross-helicity $H^C(t)$, since it is negligible when compared to the total magnetic and kinetic energy. Indeed, this correlation, initially equal to zero, reaches a maximum value of 0.081 for the DNS run, and of 0.069 for the LES MHD II run, to respectvely finish at a value of 0.051 and 0.056.

We now investigate the spectral behavior of our LES model by comparing the DNS and LES MHD II kinetic and magnetic energy spectra at various dynamical times.

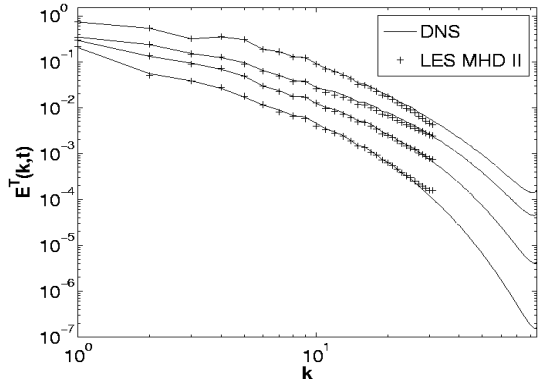

FIG. 5: Total energy spectra $E^T(k) = E^M(k) + E^V(k)$, at time $t = 1$, $t = 3$, $t = 5$, and $t = 10$ from top to bottom, for runs **I** (256^3 DNS solid line), and **III** (64^3 LES MHD II +).

Figure 5 shows the total (kinetic plus magnetic) energy spectra $E^T(k) = E^M(k) + E^V(k)$ at times $t = 1$, $t = 3$, $t = 5$, and $t = 10$ obtained from DNS and LES MHD II computations. At any wavenumber and at any time, our LES MHD II model reproduces more correctly the DNS spectra than the LES MHD I does (see Fig. 1). It is clear that the spectral over-estimations at small scales obtained with this latter model is cured by the new formulation of the eddy-damping rates.

VII. RANDOM FLOW AT $P_M = 0.1$

Since the new eddy-damping times involved in our LES MHD II model allow for a more refined differenciation between the magnetic diffusivity and the kinematic viscosity, we simulated a flow at a magnetic Prandtl number less than unity, namely $P_M = 0.1$. In order to highlight the efficiency of the new damping times to reproduce the flow dynamics, we compared both the LES MHD I and II data against the DNS results. For these simulations we kept identical flow initial conditions as in the previous section. A first comparison between the time evolution of the kinetic and magnetic energies computed from a DNS, and a simulation using the LES MHD II model, is plotted in Figure 6.

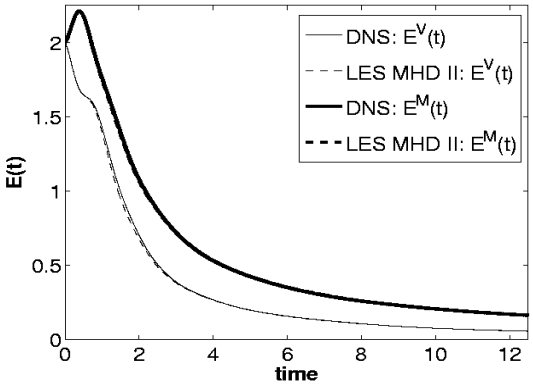

FIG. 6: Total kinetic and magnetic energy temporal evolution, for runs **IV** (256^3 DNS), and **V** (64^3 LES MHD II) at a magnetic Prandtl number of 0.1

One can observe that the model almost reproduces the exact temporal evolution of both kinetic and magnetic energy. The evolution of the kinetic and magnetic helicities (not shown) is also well-reproduced by the model. Once again, the cross-correlation remains weak all along the simulations; initially equal to zero, it reaches a maximum value of 0.056 for the DNS, 0.057 for the LES MHD I, and 0.057 for the LES MHD II runs, before respective final values of 0.044 (DNS), 0.046 (LES MHD I), and 0.045 (LES MHD II).

We now present in Figure. 7 the total (kinetic plus magnetic) energy spectra evolution at times $t = 1$, $t = 3$, $t = 5$, and $t = 10$, obtained from DNS, LES MHD I, and LES MHD II data. Although at small wavenumbers both LES models correctly reproduce the DNS spectra, at large wavenumbers, strong differences appear among these various spectra. Indeed, the LES MHD II results slightly underestimate this range of the DNS spectra, whereas the LES MHD I highly overestimates it.

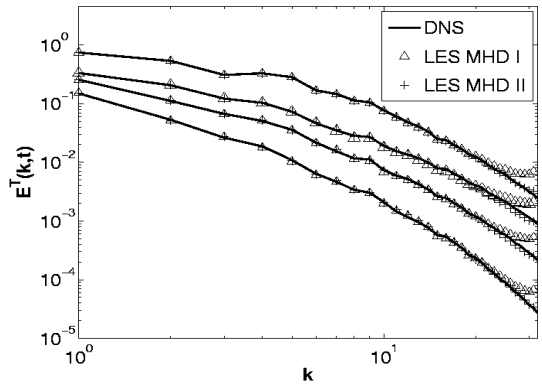

FIG. 7: Total energy spectra, at times $t = 1$, $t = 3$, $t = 5$, and $t = 10$ from top to bottom, for runs **IV** (256^3 DNS, solid line), **V** (64^3 LES MHD II, plusses), and **VI** (64^3 LES MHD I, triangles) at $P_M = 0.1$.

VIII. DETERMINISTIC ORSZAG-TANG FLOW AT $P_M = 1$

For a majority of flows, the correlation between the velocity and the magnetic field (or cross-helicity) is non negligible, leading to a slowed-down dynamics and energy spectra depending on the amount of correlation in the flow [29]. It has also been observed that local patches of either aligned or anti-aligned velocity-magnetic field configurations can be found both in the solar wind and in numerical simulations [27, 28]. We therefore decided to evaluate the ability of our model to treat a flow with strong cross-correlation by examining the evolution of the so-called three-dimensional Orszag-Tang flow with an initial global correlation $H^C(t = 0) = 1.63$ (to be compared with the total kinetic and magnetic energy $E^V(t = 0) = E^M(t = 0) = 2$).

A. Global quantities

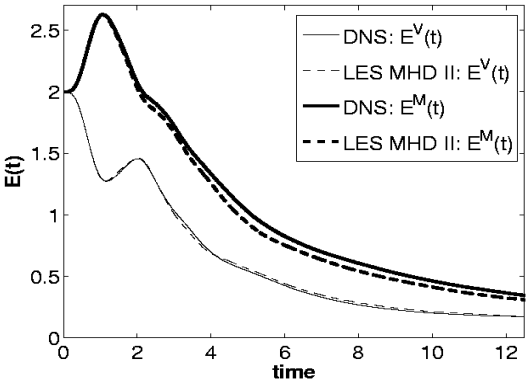

FIG. 8: Kinetic and magnetic energy evolution, for runs **VII** (256^3 DNS solid line), and **VIII** (64^3 LES MHD II dashed line) with non-zero velocity-magnetic field correlation.

The kinetic energy evaluated with the LES MHD II fits with great accuracy to the kinetic energy obtained with the DNS (see Fig. 8); however, the magnetic energy which is well-reproduced until $t = 2$ departs measurably from the DNS data after this time.

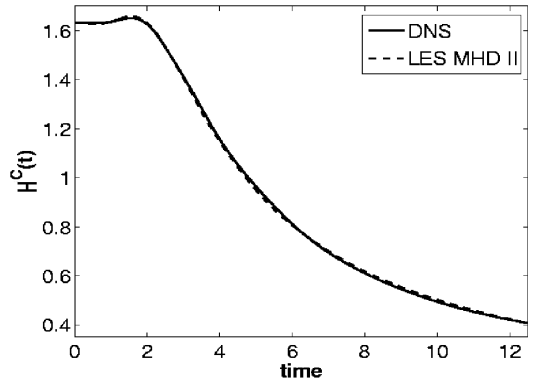

FIG. 9: Global velocity-magnetic field cross correlation, for runs **VII** (256^3 DNS straight line), and **VIII** (64^3 LES MHD II dashed line).

The global cross-correlation, computed from either DNS or LES MHD II data, are quite close (see Fig. 9), demonstrating that although the model does not explicitly take this quantity into account, it still maintains a reliable evolution for it. However, the well-known temporal growth of the normalized cross-correlation coefficient $\rho(t) = H^C(t)/(E^V(t) + E^M(t))$ shown in Fig. 10 is not represented as accurately as either E_T or H^C. This could be tentatively attributed to the fact that turbulent transport coefficients based on the velocity-magnetic field correlation itself would emerge from a complete model (as derived in [1], see also [26]) the effect of which might be to dampen the correlation growth over time. Note that this discrepancy likely emerges from the less accurate representation of the magnetic energy itself, as displayed in Fig. 8.

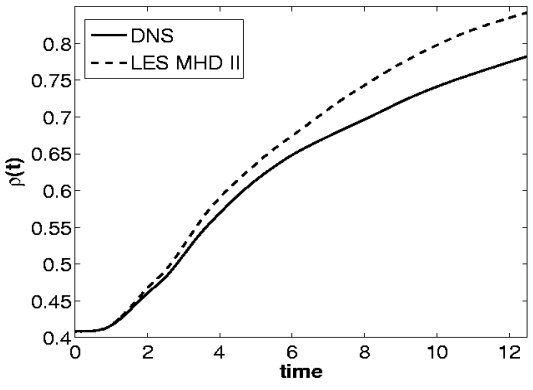

FIG. 10: Correlation coefficient $\rho(t)$, for runs **VII** (256^3 DNS solid line), and **VIII** (64^3 LES MHD II dashed line).

B. Spectral features

We finally investigate the spectral behavior of our model on this particular Orszag-Tang flow. We respectively plot in Fig. 11 and Fig. 12 the kinetic and magnetic spectra of both DNS and LES MHD II, at times $t = 1$, $t = 3$, $t = 5$, and $t = 10$.

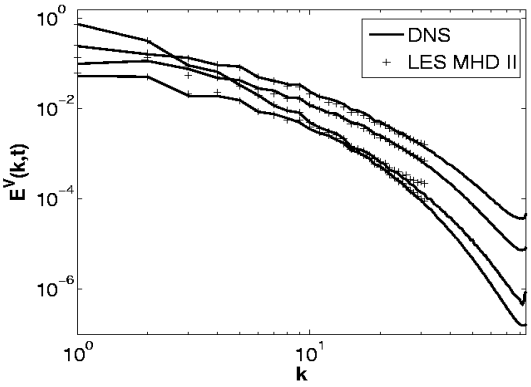

FIG. 11: Kinetic energy spectra, at times $t = 1$, $t = 3$, $t = 5$, and $t = 10$ from up to down, for data **VII** (256^3 DNS straight line), and **VIII** (64^3 LES MHD II plusses).

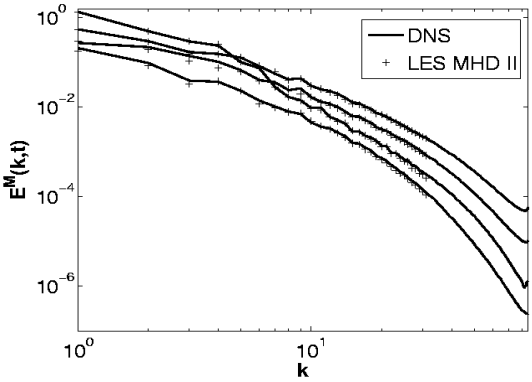

FIG. 12: Same as Fig. 11 for magnetic energy spectra.

One can observe strong similarities of the modeled spectra with the directly simulated ones, although small differences appear at large scales.

In order to evaluate the effect of the model on the cross-correlation, scale by scale, we represented in Fig. 13 its spectra at times $t = 3$ and $t = 10$ (we show only two times for readability purpose).

We can observe that at large scales which are the most energetic, the model reproduces correctly the spectra obtained with the DNS at both times. But, close to the cut-off, the model strongly under-estimates the cross-correlation. This phenomenon, as stated before, is linked to the eddy viscosity and eddy diffusivity which dissipate the kinetic and magnetic resolved scales, as well as the cross-correlation at these scales. The reconstruction procedure allows to reinject energy and helicity (when taken into account) at these scales, but not the correlation.

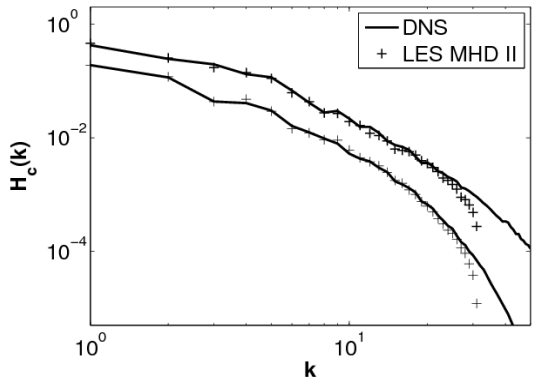

FIG. 13: Correlation spectra at $t = 3$ (top) and $t = 10$ (bottom), for data **VII** (256^3 DNS straight line), and **VIII** (64^3 LES MHD II +).

IX. CONCLUSION

In this paper we accomplish two complementary tasks. We first develop a LES for MHD using the EDQNM equations and transport coefficients derived in [23] but in the non-helical case. We then show that not all relevant time scales appearing in the cumulant expansions of the primitive MHD equations are taken into account in the phenomenological formulation of [23]. Indeed, one can derive several new eddy-damping times for the EDQNM equations, and document how, by using them, one can considerably improve the treatment of the magnetic and kinetic energy transfers in the Large Eddy Simulation approach taken in this paper.

A possible extension of this work is to be able to incorporate the effect of either cross-helicity [26] and of kinetic and magnetic helicity [23] in the evaluation of eddy viscosities and eddy noise. The fact that the modeling algorithm does not depend on a specified inertial index may also be of some help in the case of a high velocity-magnetic field correlation when different spectra emerge at high values of the (normalized) H^C cross-helicity [29].

Furthermore, with such a model many astrophysical and geophysical flows can be studied and perhaps more importantly a vast range of parameters, in particular the magnetic Prandtl number, can be examined. Among such problems, the generation of magnetic fields at either low or high magnetic Prandtl number is of prime importance, in particular in the former case in view of a set of laboratory experiments studying this effect [30].

Acknowledgments

This work is supported by INSU/PNST and PCMI Programs and CNRS/GdR Dynamo. Computation time was provided by IDRIS (CNRS) Grant No. 070597, and SIGAMM mesocenter (OCA/University Nice-Sophia).

APPENDIX A: EDQNM CLOSURE

For completeness, we recall here the expression of the EDQNM closure equations for the magnetic and kinetic energy without helicity. The first non-helical EDQNM equations were first derived in [22] but we follow here the notation of [23] which gives the free helical closure:

$$(\partial_t + 2\nu k^2)E^V(k,t) = \widehat{T}^V(k,t) \quad \text{(A1)}$$

$$(\partial_t + 2\eta k^2)E^M(k,t) = \widehat{T}^M(k,t) \quad \text{(A2)}$$

where the nonlinear transfer terms for the kinetic and magnetic energy, respectively $\widehat{T}^V(k,t)$ and $\widehat{T}^M(k,t)$ are expressed as:

$$\widehat{T}^V(k,t) = \iint_{\Delta_k} \theta_{_{kpq}}(t) S^V(k,p,q,t) dpdq \ , \quad \text{(A3)}$$

$$\widehat{T}^M(k,t) = \iint_{\Delta_k} \theta_{_{kpq}}(t) S^M(k,p,q,t) dpdq \ . \quad \text{(A4)}$$

Here Δ_k is the integration domain with p and q such that (k,p,q) form a triangle, and $\theta_{_{kpq}}(t)$ namely the triad-relaxation time is expressed as:

$$\theta_{kpq}(t) = \frac{1 - e^{-\mu_{kpq}t}}{\mu_{kpq}} \ , \quad \text{(A5)}$$

with $\mu_{kpq} = \mu_k + \mu_p + \mu_q$ where the μ_k's are called eddy-damping rates and read:

$$\mu_k = +\lambda \left(\int_0^k q^2 (E_q^V + E_q^M) dq \right)^{\frac{1}{2}} + \sqrt{\frac{2}{3}} k \left(\int_0^k E_q^M dq \right)^{\frac{1}{2}} + (\nu + \eta) k^2. \quad \text{(A6)}$$

The constant λ can be expressed as a function of the Kolmogorov constant C_k appearing in front of the kinetic energy spectrum such that:

$$\lambda = 0.218 C_k^{\frac{3}{2}} \ , \quad \text{(A7)}$$

following [18].

The expressions of $S^V(k,p,q,t)$ and $S^M(k,p,q,t)$ can be further explicited (with the time dependency of magnetic and kinetic energy spectra omitted here) as :

$$\begin{aligned} S^V(k,p,q,t) &= \frac{k}{pq} b_{kpq} \left[k^2 E^V(q) E^V(p) - p^2 E^V(q) E^V(k) \right] \\ &+ \frac{k}{pq} c_{kpq} \left[k^2 E^M(q) E^M(p) - p^2 E^M(q) E^V(k) \right] \\ &= S_1^V(k,p,q,t) + S_2^V(k,p,q,t) \\ &+ S_3^V(k,p,q,t) + S_4^V(k,p,q,t) \ . \end{aligned} \quad \text{(A8)}$$

$$\begin{aligned} S^M(k,p,q,t) &= \frac{k}{pq} h_{kpq} \left[k^2 E^M(p) E^V(q) - p^2 E^V(q) E^M(k) \right] \\ &+ \frac{k^3}{pq} c_{kpq} \left[\frac{k^2}{p^2} E^V(p) E^M(q) - E^M(q) E^M(k) \right] \\ &= S_1^M(k,p,q,t) + S_2^M(k,p,q,t) \\ &+ S_3^M(k,p,q,t) + S_4^M(k,p,q,t) \ . \end{aligned} \quad \text{(A9)}$$

In Eqs. (A8) and (A9) the geometric coefficients b_{kpq}, c_{kpq}, and h_{kpq} are defined as:

$$\begin{aligned} b_{kpq} &= pk^{-1}(xy+z^3), \quad c_{kpq} = pk^{-1}z(1-y^2) \ , \\ h_{kpq} &= z(1-y^2) \ , \end{aligned}$$

where x, y, z are the cosine of the interior angles opposite to $\mathbf{k}, \mathbf{p}, \mathbf{q}$. This completes the description of the EDQNM closure for MHD as developed in [22, 23]. The helical case, dealt with in [21] for a pure fluid and in [23] from the EDQNM standpoint, will be studied in a forthcoming paper when coupling to a magnetic field is involved.

APPENDIX B: A MORE GENERAL EDDY DAMPING

In [23], the eddy damping term is built on a phenomenological ground; namely, one argued about the necessity of introducing the Alfvén time scale in the damping coefficient, without actually referring to the set of cumulant expansion equations. This change alone, from a traditional hydrodynamic EDQNM closure, led to energy spectra that differ from the Kolmogorov case, with a $k^{-3/2}$ law in the uncorrelated case, and with a $E^{\pm}(k) \sim k^{-m^{\pm}}$ in the correlated case [1], with $m^+ + m^- = 3$; here, $E^{\pm}(k)$ are the energy spectra of the Elsässer variables $\mathbf{z}^{\pm} = \mathbf{v} \pm \mathbf{b}$.

However, when examining the succession of equations for the higher-order moments, and keeping the total correlation between the velocity and the magnetic field equal to zero to simplify the algebra, a more complex structure emerges, which may help the modeling of the MHD dynamics to be closer to the DNS than the results shown in Fig.1. There are in fact four groups of terms in the closure equations. The first group corresponds to the pure fluid case and can be written symbolically as:

$$\left(\frac{\partial}{\partial t} + \nu(k^2+p^2+q^2)\right) < uuu > \simeq k < uuuu > \ . \tag{B1}$$

This leads, as usual, to two characteristic times written here as: $\tau_D^{VV} = \left(\nu(k^2+p^2+q^2)\right)^{-1}$ and $\tau_{NL} = (ku)^{-1}$. The second group writes symbolically again as:

$$\left(\frac{\partial}{\partial t} + \nu k^2 + \eta(p^2+q^2)\right) < uuu > \tag{B2}$$

$$\simeq k < uuuu > + k < bbuu > \ .$$

Here, two new times can be extracted, namely a dissipative time $\tau_D^{VM} = \left(\nu k^2 + \eta(p^2+q^2)\right)^{-1}$, and $\widetilde{\tau}_A = u(kbb)^{-1}$, a modified Alfvén time.

The third group of closure terms is of the following type:

$$\left(\frac{\partial}{\partial t} + (\eta k^2 + \eta p^2 + \nu q^2)\right) < bbu > \tag{B3}$$

$$\simeq k < bbbb > + k < bbuu > \ .$$

and finally the fourth group:

$$\left(\frac{\partial}{\partial t} + (\eta k^2 + \nu p^2 + \eta q^2)\right) < bbu > \tag{B4}$$

$$\simeq k < bbbb > + k < bbuu > \ .$$

Again, the following new characteristic dissipative times can be a priori deduced from these two groups (with similar nomenclatures as before): $\tau_D^{MM} = \left(\eta k^2 + \eta p^2 + \nu q^2\right)^{-1}$, and $\tau_D^{MV} = \left(\eta k^2 + \nu p^2 + \eta q^2\right)^{-1}$.

In conclusion, a careful examination of the cumulant equations has led to the adjunction of several new times, distinguishing between magnetic and kinetic energy transfer as well as the different quantities entering the transfer terms.

Note that the new modified Alfvén time is finally expressed as:

$$\widetilde{\tau}_A^{-1}(k) = C_A \left(\frac{\int_0^k E^M(q)dq}{\int_0^k E^V(q)dq}\right)^{\frac{1}{2}} \left[\int_0^k q^2 E^M(q)dq\right]^{\frac{1}{2}} \ . \tag{B5}$$

It incorporates the lack of equipartition between the kinetic and magnetic energy that is often observed, and this for example should also alter the dynamics, in the early (kinematic) phase of the dynamo problem. The non-linear time has the classical expression built only on the velocity field:

$$\tau_{NL}^{-1}(k) = \lambda \left[\int_0^k q^2 E^V(q)dq\right]^{\frac{1}{2}} \ . \tag{B6}$$

Finally, we numerically estimated the value of the Alfvén time constant $C_A = 0.8$. This point will need further study as we extend the number of flows that are tested with this LES. The constant λ is determined through the relation [A7] in Appendix A. The model has thus two open parameters that can be evaluated once the constants appearing in front of the energy spectra in MHD are determined.

Also note that the way the dissipation coefficients are taken into account may well affect the results when the magnetic Prandtl number differs substantially from unity unless possibly when both the kinetic and magnetic Reynolds numbers are very large because of the effect of renormalisation of transport coefficients [31].

Similarly to equation (A5) for the eddy damping rate in [23], we define generalized rates as:

$$\theta_{kpq}^{XY}(t) = \frac{1 - e^{-\mu_{kpq}^{XY} t}}{\mu_{kpq}^{XY}} \ , \tag{B7}$$

with $\mu_{kpq}^{XY} = \mu_k^{XY} + \mu_p^{XY} + \mu_q^{XY}$ and with XY standing for either VV, VM, MV or MM and with:

$$\mu_k^{VV} = \left(\tau_D^{VV}(k)\right)^{-1} + \left(\tau_{NL}(k)\right)^{-1} \ , \tag{B8}$$

$$\mu_k^{VM} = \left(\tau_D^{VM}(k)\right)^{-1} + \left(\tau_{NL}(k)\right)^{-1} + \left(\widetilde{\tau}_A(k)\right)^{-1} \ , \quad \text{(B9)}$$

$$\mu_k^{MV} = \left(\tau_D^{MV}(k)\right)^{-1} + \left(\tau_{NL}(k)\right)^{-1} + \left(\widetilde{\tau}_A(k)\right)^{-1} \ , \quad \text{(B10)}$$

and

$$\mu_k^{MM} = \left(\tau_D^{MM}(k)\right)^{-1} + \left(\tau_{NL}(k)\right)^{-1} + \left(\widetilde{\tau}_A(k)\right)^{-1} \ . \quad \text{(B11)}$$

[1] R. Grappin, J. Léorat and A. Pouquet, Astron. Astrophys. **123**, 51 (1983).

[2] W.H. Matthaeus, and M.L. Goldstein, J. Geophys. Res. **87**, 6011 (1982).

[3] P. Iroshnikov Sov. Astron. **7**, 566 (1963); R. H. Kraichnan Phys. Fluids **8**, 1385 (1965)

[4] J. Maron and P. Goldreich, Astrophys. J. **554**, 1175 (2001).

[5] W. C. Müller and R. Grappin, Phys. Rev. Lett. **95** 114502 (2005).

[6] P.D. Mininni and A. Pouquet, Physical Review Letters **99**, 254502 (2007).

[7] J. Podesta, D. Roberts and M. Goldstein, Astrophys. J. **664**, 543 (2007).

[8] K. Yoshida and T. Arimitsu Phys. Fluids. **19**, 045106 (2007)

[9] S. Galtier, S. Nazarenko, A. C. Newell and A. Pouquet, J. Plasma Phys. **63**, 447 (2000)

[10] J. Saur, H. Politano, A. Pouquet, and W. Matthaeus, A & A, **386**, 699 (2002).

[11] See the special issue on MHD dynamo experiments in *Magnetohydrodynamics* **38** (2002).

[12] N.L. Peffley, A.B. Cawthorne, D.P. Lathrop, Phys. Rev. E **61**, 5287 (2000).

[13] M. Bourgoin, L. Marie, F. Pétŕelis, C. Gasquet, A. Guigon, J.B. Luciani, M. Moulin, J. Namer, A. Burguete, Chiffaudel, F. Daviaud, S. Fauve, P. Odier, and J.-F. Pinton, Phys. Fluids **14**, 3046 (2002).

[14] F. Pétrélis, M. Bourgoin, L. Marié, J. Burguete, A. Chiffaudel, F. Daviaud, S. Fauve, P. Odier, and J.-F. Pinton, Phys. Rev. Lett. **90**, 174501 (2003).

[15] Y. Ponty, H. Politano and J.F. Pinton, Phys. Rev. Lett. **92**, 144503 (2004).

[16] Y. Ponty, P.D. Mininni, D.C. Montgomery, J-F. Pinton, H. Politano, and A. Pouquet, Phys. Rev. Lett. **94** 164502 (2005).

[17] P. Mininni, A. Pouquet and P. Sullivan, "Two examples from geophysical and astrophysical turbulence on modeling disparate scale interactions," Summer school on mathematics in geophysics, Roger Temam and Joe Tribbia Eds., Springer Verlag, to appear (2008).

[18] J.-P. Chollet and M. Lesieur, Journal of Atmospheric Sciences **38**, 2747 (1981)

[19] E. Parker, in *Cosmical Magnetic Fields: their origin and their activity*, (New-York: Oxford University Press, 1979).

[20] H.K. Moffatt, in *Magnetic Field Generation in Electrically Conducting Fluids*, (Cambridge Univ. Press, Cambridge, U.K., 1978).

[21] J. Baerenzung, H. Politano, Y. Ponty, and A. Pouquet, to appear, Phys. Rev. E (2008).

[22] R. H. Kraichnan and S. Nagarajan, Physics of Fluids **10**, 859 (1967)

[23] A. Pouquet, U. Frisch, and J. Léorat, J. Fluid Mech. **77**, 321 (1976).

[24] A. Pouquet, " *Magnetohydrodynamic Turbulence*," Les Houches Summer School on Astrophysical Fluid Dynamics, Session **XLVII**, 139; Eds. J. P. Zahn & J. Zinn–Justin, Elsevier (1993).

[25] J. Baerenzung, Thèse d'Etat, Observatoire de la Côte d'Azur (2008).

[26] R. Grappin, U. Frisch, J. Léorat and A. Pouquet, Astron. Astrophys. **105**, 6 (1982)

[27] M. Meneguzzi, H. Politano, A. Pouquet and M. Zolver, J. Comp. Phys. **123**, 32 (1996)

[28] W. H. Matthaeus, A. Pouquet, P. D. Mininni, P. Dmitruk, and B. Breech, preprint arXiv:0708.0801 (2007).

[29] A. Pouquet, P. L. Sulem and M. Meneguzzi Phys. Fluids, **31**, 2635 (1988)

[30] R. Monchaux, M. Berhanu, M. Bourgoin, M. Moulin, P. Odier, J.-F. Pinton, R. Volk, S. Fauve, N. Mordant, F. Pétrélis, A. Chiffaudel, F. Daviaud, B. Dubrulle, C. Gasquet, L. Marié and F. Ravelet, Phys. Rev. Lett. **98**, 044502 (2007).

[31] J. D. Fournier, P. L. Sulem and A. Pouquet, J. Phys. A **15**, 1393 (1982)